

Supporting Information

Novel hierarchical porous Fe₂O₃@GA composite for solar-Fenton catalysis of dyes

Xiaomei Li ^{a,b}, Jun Qin ^b, Xiao Zhang ^b, Yu Zhang ^b, Zhixiong Liu ^b, Jianfeng Jia ^{a*},
Haishun Wu ^a, Feng Feng ^{a,c*}, Yunfeng Bai ^b

^a School of Chemical and Material Science, Shanxi Normal University, Taiyuan
030006, China

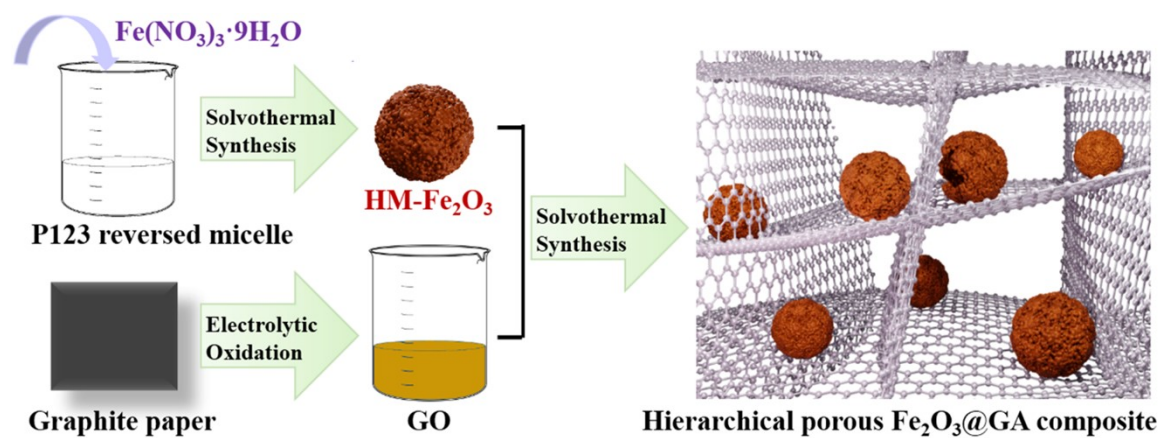
^b College of Chemistry and Chemical Engineering, Shanxi Datong University, Datong
037009, China

^c Department of Energy Chemistry and Materials Engineering, Shanxi Institute of
Energy, Taiyuan 030600, China

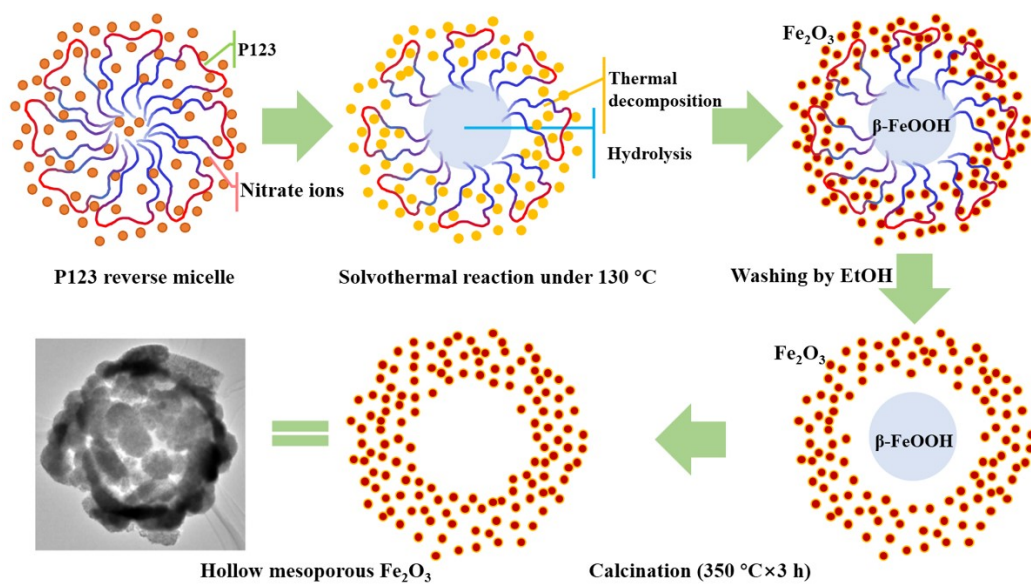
Corresponding authors.

E-mail: jjajf@dns.sxnu.edu.cn (J. Jia), feng-feng64@263.net (F. Feng)

Section A: Additional Schemes



Scheme S1 Synthesis process of hierarchical porous composite.



Scheme S2 Formation mechanism of HM- Fe_2O_3 .

Section B: Additional Texts

Text S1

Synthesis of GO

The dried graphite paper was fixed at the anode of the electrolytic cell and immersed into concentrated sulfuric acid for pre-intercalation under +1.5 V voltage. Subsequently, the intercalated graphite paper, which was 8~10 times thicker than the original, was slowly dipped into 50 % (m/m) sulfuric acid electrolyte as a sacrificial anode for electrolytic oxidation under +7 V voltage. In the electrolytic oxidation reaction, the sufficiently oxidized GO was continuously peeled off into the sulfuric acid electrolyte, separated by filtration and repeatedly cleaned with deionized water. Finally, the GO was ultrasonically dispersed into water to form a homogeneous dispersion (~15 mg/mL) for further use.

Text S2

Formation mechanism of HM-Fe₂O₃

The formation mechanism of HM-Fe₂O₃ was proposed in Scheme S2. First, P123 reverse micelles formed in n-butanol solution after sufficient uniform stirring. The micelle has a relatively stable spherical morphology, the core of which was formed by the hydrophilic block of P123 and a small amount of water, and the hydrophobic block of P123 formed the outer structure. Iron species were well dispersed around the reverse micellar with the assistance of n-butanol and HNO₃. Second, when the micellar mixture was transferred to a solvothermal reaction under 130 °C, the nitrate began to decompose gradually to form Fe₂O₃ grains, aggregating into loose secondary particles. Slow hydrolysis also occurred inside the hydrophilic core to produce β-FeOOH. Thus, a relatively stable intermediate composed of Fe₂O₃-P123 shell and β-FeOOH core formed. Third, the intermediate was washed and calcined to remove P123 and NO_x, and β-FeOOH gradually decomposed into Fe₂O₃ and fused into the shell to form hollow

Fe₂O₃ spheres. During the continuous calcination, the mesopores in Fe₂O₃ particles opened with the removal of micelles.

To verify the correlation between nitrate decomposition and Fe₂O₃ formation mentioned above. Fe(NO₃)₃·9H₂O was replaced by FeCl₃·6H₂O for comparison, and no precipitate was found after the solvothermal reaction. The supernatant after the solvothermal reaction was tested by UV-Vis absorption, and the characteristic band of NO_x at 320–400 nm proved the decomposition of nitrate (**Fig. S4**). XRD pattern (**Fig. S5**) of the intermediate mentioned above shows the characteristic peaks of both Fe₂O₃ and β-FeOOH (JCPDS NO. 75-1594), suggesting the formation of β-FeOOH. The intermediate's SEM image (**Fig. S6**) exhibits the flocculent loose β-FeOOH structure inside the Fe₂O₃ shell. These tests prove that the formation process of HM-Fe₂O₃ materials includes the above three stages.

Section C: Additional Figures

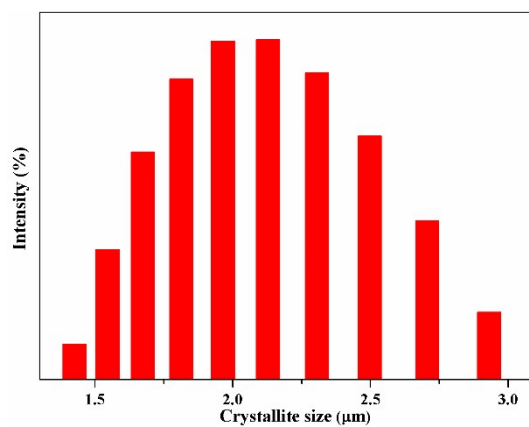


Fig. S1. Size distribution of HM-Fe₂O₃.

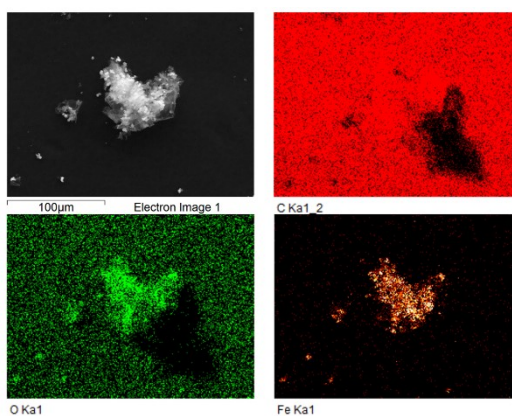


Fig. S2. EDX element mappings of H-Fe₂O₃@GA composite.

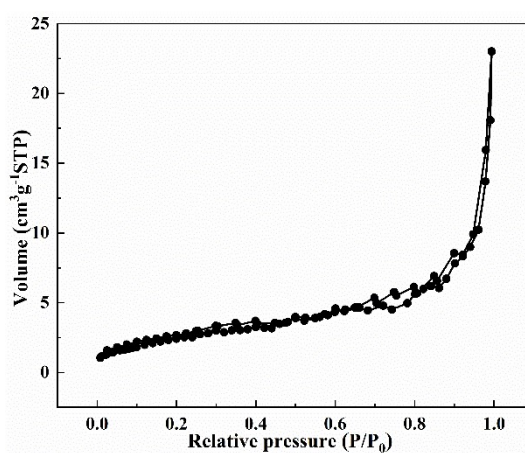


Fig. S3. N₂-adsorption-desorption isotherms of R-Fe₂O₃.

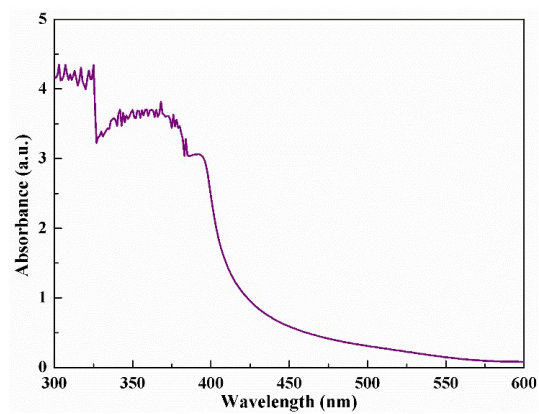


Fig. S4. UV-Vis spectra of the reaction solution after solvothermal reaction.

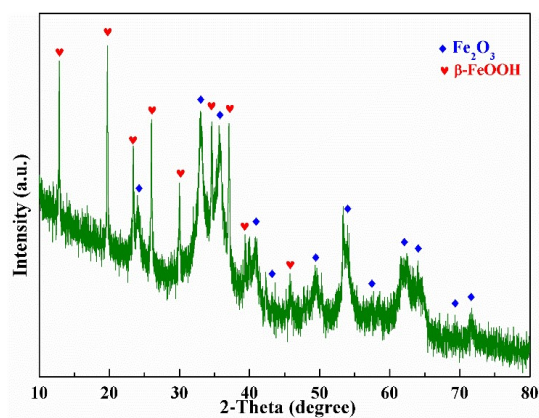


Fig. S5. Wide-angle XRD pattern of the product before calcination.

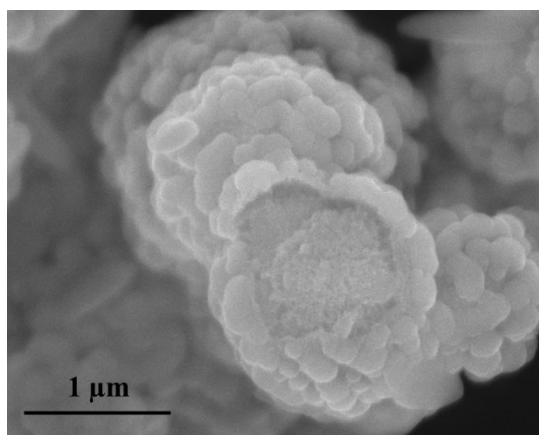


Fig. S6. SEM image of the product of solvothermal reaction before calcination.

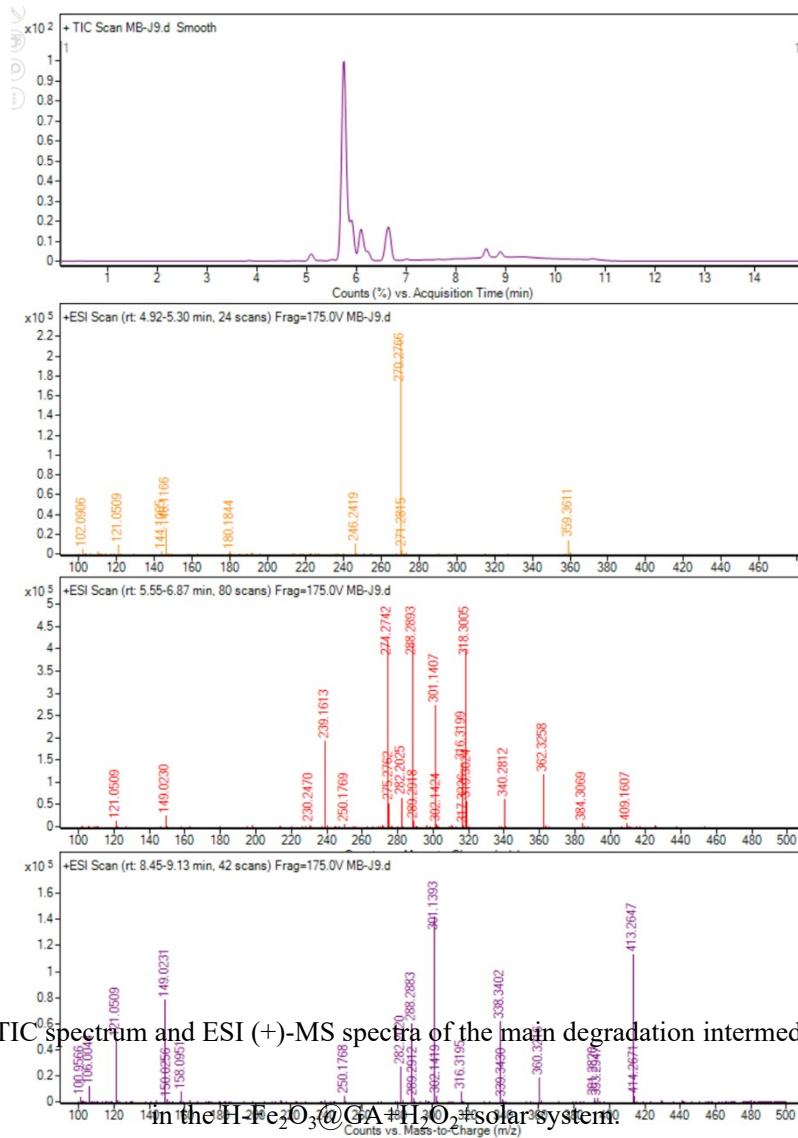


Fig. S7. LC-TIC spectrum and ESI (+)-MS spectra of the main degradation intermediates of MB in the $\text{H-Fe}_2\text{O}_3@\text{GA}+\text{H}_2\text{O}_2$ solar system.

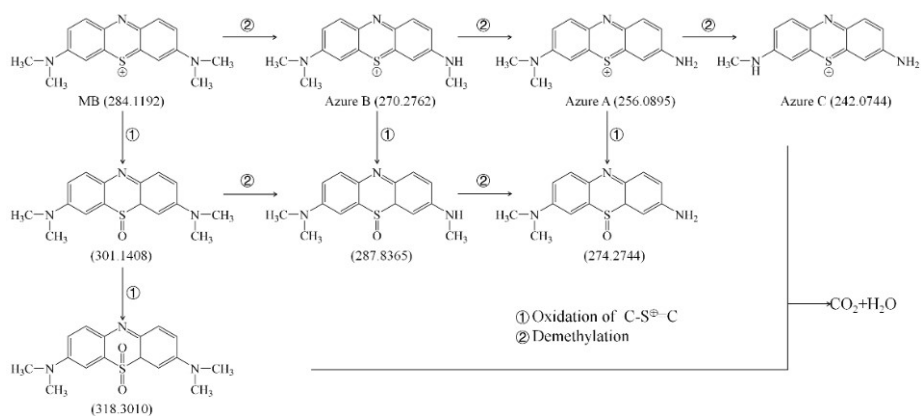


Fig. S8. Proposed degradation pathway of MB in $\text{H-Fe}_2\text{O}_3@\text{GA}+\text{H}_2\text{O}_2$ solar system.

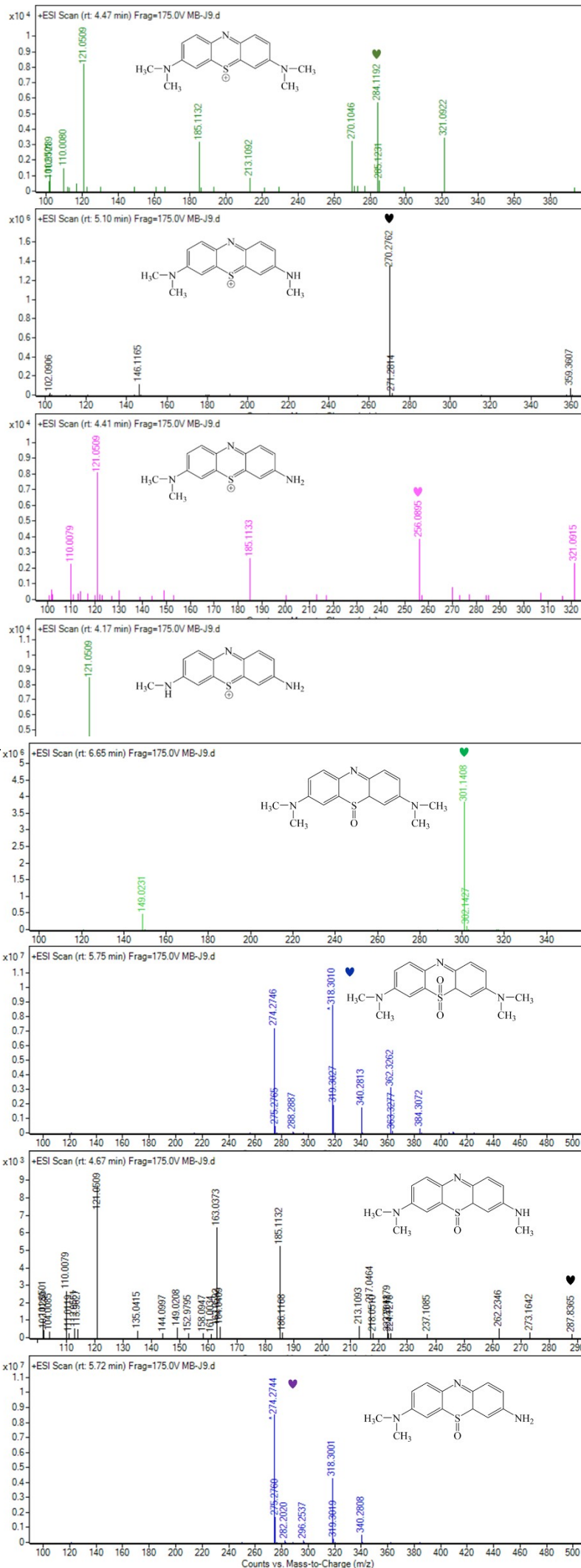


Fig. S9. T

lation.

Fig. S10. The ESI (+)-MS spectra of degradation intermediates of MB by oxidation of C=S⁺-C groups.

Section D: Additional Tables

Table S1. Structural parameters of materials on BET.

Materials	Surface area (m ² /g)	Pore volume (cm ³ /g)	Pore size (nm)
HM-Fe ₂ O ₃	43.69	0.18	11.72
GA	38.76	0.15	14.10
H-Fe ₂ O ₃ @GA-30%	37.50	0.12	14.36
H-Fe ₂ O ₃ @GA-43%	30.67	0.12	10.68
H-Fe ₂ O ₃ @GA-58%	35.16	0.14	12.21
R-Fe ₂ O ₃	7.88	0.03	15.59

Table S2. Removal efficiency and the first-order reaction rate constant of MB under different conditions.

Reaction condition	$\eta/\%$	K/min^{-1}	R^2
H-Fe ₂ O ₃ @GA+H ₂ O ₂ +solar	91.8	0.0314	0.9522

H-Fe ₂ O ₃ @GA+H ₂ O ₂ +dark	43.2	0.0048	0.8566
H-Fe ₂ O ₃ @GA+solar	55.6	0.0080	0.9769
H-Fe ₂ O ₃ @GA+dark	23.6	0.0015	0.6917
HM-Fe ₂ O ₃ +H ₂ O ₂ +solar	46.5	0.0061	0.9633
R-Fe ₂ O ₃ + H ₂ O ₂ +solar	39.3	0.0046	0.9352
H ₂ O ₂ +solar	6.5	0.0005	0.9770
Solar	5.4	0.0006	0.8131

Table S3. Removal efficiency and the first-order reaction rate constant of MB under different initial MB concentrations, H₂O₂ dosages, pHs, and Fe₂O₃ contents.

Variations	Concentration	$\eta/\%$	K/min^{-1}	R^2
MB concentration	20 mg/L	97.5	0.0428	0.9145
	30 mg/L	95.3	0.0387	0.9148
	40 mg/L	95.1	0.0353	0.9882
	50 mg/L	91.8	0.0312	0.9445
H ₂ O ₂	0.4 mM	95.1	0.0353	0.9882
	0.7 mM	95.4	0.0336	0.9726
	1.0 mM	96.3	0.0372	0.9812
	2.0 mM	95.8	0.0370	0.9949
pH	3.02	96.4	0.0350	0.9165
	7.08	95.1	0.0353	0.9882
	10.20	88.5	0.0243	0.9266
Fe ₂ O ₃ content	30%	75.7	0.0161	0.9879

43%	95.1	0.0353	0.9882
58%	81.5	0.0184	0.9585
